International Journal of Geosciences, 2026, 17(8), 525-547
https://www.scirp.org/journal/ijg
ISSN Online: 2156-8367
ISSN Print: 2156-8359

Petrographic and Geochemical Studies of the Lavas from the Southern Part of Anjouan Island, Comoros Archipelago: Geodynamic Implication

Ali Rachidi Oikifou[1]*, Ibrahima Labou[2], Samba Cissokho[1], Mahamadane Diene[2], Ahamada Adinane[1]

[1]Departement of Geology, Faculty of Sciences and Technics, Cheikh Anta Diop University, Dakar, Senegal
[2]National Superior School of Mines and Geology, Cheikh Anta Diop University, Dakar, Senegal
Email: *oikifoualirachidi@gmail.com, alirachidi.oikifou@ucad.edu.sn

How to cite this paper: Oikifou, A.R., Labou, I., Cissokho, S., Diene, M. and Adinane, A. (2026) Petrographic and Geochemical Studies of the Lavas from the Southern Part of Anjouan Island, Comoros Archipelago: Geodynamic Implication. *International Journal of Geosciences*, **17**, 525-547.
https://doi.org/10.4236/ijg.2026.178025

Received: June 8, 2026
Accepted: August 1, 2026
Published: August 4, 2026

Abstract

Petrographic and geochemical investigations of the southern part of Anjouan Island (Comores archipelago) reveal a diversity of volcanic facies, including alkaline basalts, basanites, phonolitic nephelinites, and phonolites. Petrography analysis highlights the occurrence of both vesicular and non-vesicular structures, as well as porphyritic and fluidal microlitic textures. The mineralogical composition reflects a sequential crystallization of opaque minerals, olivine, pyroxene, sanidine, and nepheline. Geochemistry, for its part, highlights the alkaline nature and silica undersaturation of the rocks from the southern part of Anjouan Island. It also reveals magmatic differentiation of the lavas through fractional crystallization, evolving from alkaline basalts to phonolites, via basanites and phonolitic nephelinites, respectively. These lavas are also enriched in LREE and depleted in HREE with steeply sloping spectra. These geochemical characteristics are consistent with an enriched mantle source located at great depth in the lower mantle, in which garnet and amphibole occur as residual. This source, derived from a mantle plume, underwent a low degree of partial melting, generating a magma that likely ascended through lithospheric fractures associated with hotspot activity, thereby producing oceanic island basalts (OIBs); this interpretation is supported by the presence of positive Nb anomalies.

Keywords

Comoros Archipelago, Anjouan Island, Geochemistry, Enriched Mantle Source, Mantle Plume, Hotspot, Oceanic Island Basalts (OIB)

1. Introduction

Comprising four islands of volcanic origin ([1] [2]), the Comoros archipelago is located in the Mozambique Channel, between the continental blocks of Madagascar to the east and southeast and Africa to the west [3] (**Figure 1**). The islands are aligned along a WNW-ESE axis ([1] [2] [4]) and, from east to west, consist of Mayotte (the oldest), Anjouan, Moheli and Grande Comore (the youngest, with ongoing volcanic activity), as well as four associated seamounts: the Jumelles, the Zélée Banks, the Geyser, and the Leven [5].

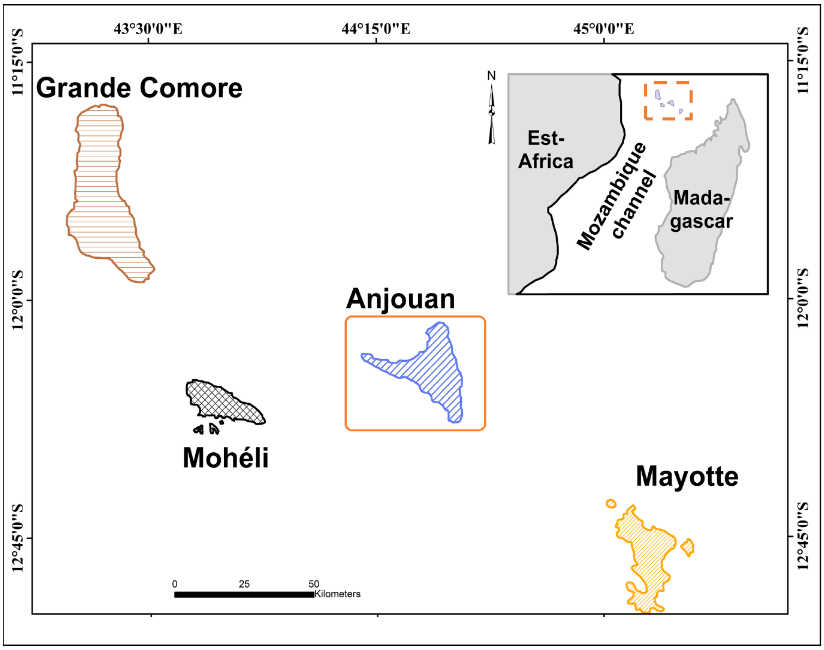

Figure 1. Map showing the location of the Comoros archipelago and Anjouan Island [3], modified.

The island of Anjouan, where the study area is located, lies in the central part of the Comoros archipelago between longitudes 44˚11' and 44˚32'E and latitudes 12˚02' and 12˚30'S (**Figure 1**). With an area of 424 km^2, Anjouan is the second-largest island in the archipelago after Grande Comore and is also the second island to have formed after Mayotte. Generally triangular in shape, the island is characterized by highly rugged topography with steep slopes. It comprises three main morphological domains [6]: (i) a high, rugged central massif deepley incised by intense erosion, reminiscent of the cirques of the Piton des Neiges massif on Réunion, (ii) a narrow coastal zone with limited plains, and (iii) three peninsulas [7], namely the Sima Peninsula to the west; the Jimilimé Peninsula to the north, and the Nioumakélé Peninsula to the south.

The islands of the Comoros Archipelago are underlain by a substratum whose nature remains debated. Several hypotheses have been proposed:

1) [8]-[12], based on the presence of detrital sedimentary enclaves within Comorian lavas, suggest that the archipelago is underlain by continental crust;

2) [13] puts forward the argument that detrital enclaves found in the archipelago are merely sediments deposited on an oceanic crust. This has been confirmed bay [14]-[18], based on geophysical data;

3) finally, [19] propose the existence of a transitional ocean-continental crust beneath the archipelago, also based on geophysical data.

Furthermore, the geotectonic setting governing magma generation in the Comoros Archipelago remains a matter of debate, and three hypotheses have been proposed:

1) [20] [21] suggest the presence of an oceanic hotspot, based on geochronological data, indicating a progressive increase in the age of volcanic activity from west to east, from Grande Comore to Mayotte;

2) [10] argues that Comorian volcanism is primarily controlled by lithospheric fractures oriented NNW-SSE and WNW-ESE. However, recent findings, including the discovery of a submarine volcano east of Mayotte [22], as well as evidence of Holocene volcanism on Anjouan in the central part of the archipelago [3] and ongoing volcanic activity at Karthala on Grande Comore in the western part of the archipelago [23], challenge the hypothesis of a simple eastward age progression.

3) finally, [24] puts forward the hypothesis that the islands of the Comoros archipelago are the emerged parts of a slaw accretion ridge.

The aim of this study is therefore to provide the first petrographic and geochemical data from the southern part of Anjouan Island in order to constrain the magma source and the geotectonic setting of the Island in particular, and to contribute to a better understanding of the geology of the Comoros archipelago in general.

2. Geological Context

2.1. General Geological Context

The Comoros archipelago consists of four volcanic islands ([1] [2]): Mayotte, Anjouan, Moheli and Grande Comore. These islands are distributed over an average distance of approximately 275 km along an ESE-WNW oriented submarine plateau ([1] [2]). Eastward, the archipelago extends into a series of banks, some of which are emergent (Glorieuses, Geyser) and others submerged (Zélée, Leven, Cordilières), located in the northern part of the Mozambique Channel. The Mozambique Channel itself represents an ancient rift that formed during the separation of the Malagasy microcontinent from the rest of Africa more than 180 million years ago [25]. In this context, [26] proposed two major stages in the tectonic evolution of the Mozambique Channel: (i) an intracontinental rifting phase, from the Permian to the Early Jurassic, leading to the separation of the Indo-Malagasy block from the supercontinent Gondwana [27]; and (ii) the opening of the Somali and Mozambique oceanic basins from the Middle Jurassic to the Early Cretaceous, through a process of oceanic accretion between ~ 150 and 120 Ma. This latter stage involved north-south crust extension along east-west-trending ridges [28], combined with decoupled activity along the Davie and Mozambique ridges.

2.2. Local Geological Context

The island of Anjouan is an extinct and largely barren volcanic island belonging to the Comoros archipelago [29]. It is generally interpreted as a central shield volcano that has been progressively eroded over time, upon which a younger Hawaiian-type rift system has been superimposed, in a N100˚ and 0˚ direction [30]. Previous studies ([29]-[32]) have shown that the island underwent different volcanic phases or periods during its formation (**Figure 2**). These are:

1) an early shield-building phase, corresponding to the initial stages of volcanism construction, during which the central massif of the island, known as the Ntringui massif, was formed. During this stage, a large circular gabbroic intrusive body was identified within a basin-shaped depression;

2) an eruptive phase along faults forming the island's three peninsulas, corresponding to the intermediate stage of volcanism;

3) and finally, a rejuvenation or erosional phase, accompanied by the emplacement of the most recent lava flows, corresponding to the island's recent volcanism.

However, it should be noted that our study area, located in the Nioumakélé region in the southern part of Anjouan island, between latitudes 12˚20'30"S and 12˚23'00"S and longitudes 44˚29'00"E and 44˚32'30"E (**Figure 2**), has never been the subject of previous studies.

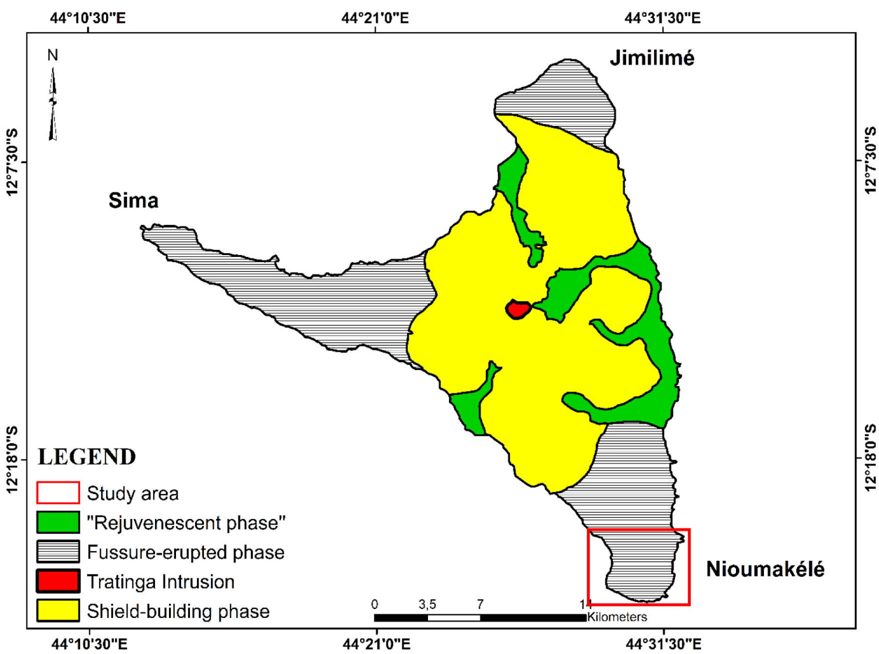

Figure 2. Geological map of Anjouan Island showing the location of the study area [29], modified.

3. Methodology

The methodology adopted in this study consists of (i) a field investigation involving petrographic and mineralogical characterization, as well as systematic sampling of the main volcanic facies outcropping in the southern part of Anjouan Island, and (ii) a laboratory study based on petrographic examination of thin sections and conventional geochemical analyses of major and trace elements.

The thin sections were prepared at the Geology Laboratory of Felix Houphouët Boigny University (Abidjan-Cocody, Côte d'Ivoire), whereas petrographic descriptions were conducted at the Petrology and Structural Geology Laboratory of Institue Fondamental d'Afrique Noire (IFAN), Cheikh Anta Diop University of Dakar (UCAD), Senegal. Geochimical analyses were performed on eleven (11) rock samples, comprising eight alkaline basalts, one basanite, one phonolitic neplelinite and one phonolite, by ACTLABS Labaratory (Canada). Major elements concentrations were determined using the Fusion-Inductively Coupled Plasma (FUS-ICP) technique, with a detection limit of 0.01wt%, while trace elements were analyzed using the FUS-ICP and Fusion Mass Spectrometry (FUS-MS).

4. Results

4.1. Lithology and Petrography

Fieldwork has identified four lithological types (**Figure 3**): alkaline basalts, basanites, phonolitic nephelinites, and phonolites, displaying both vesicular and non-vesicular structures, as well as porphyritic and fluidal microlitic textures.

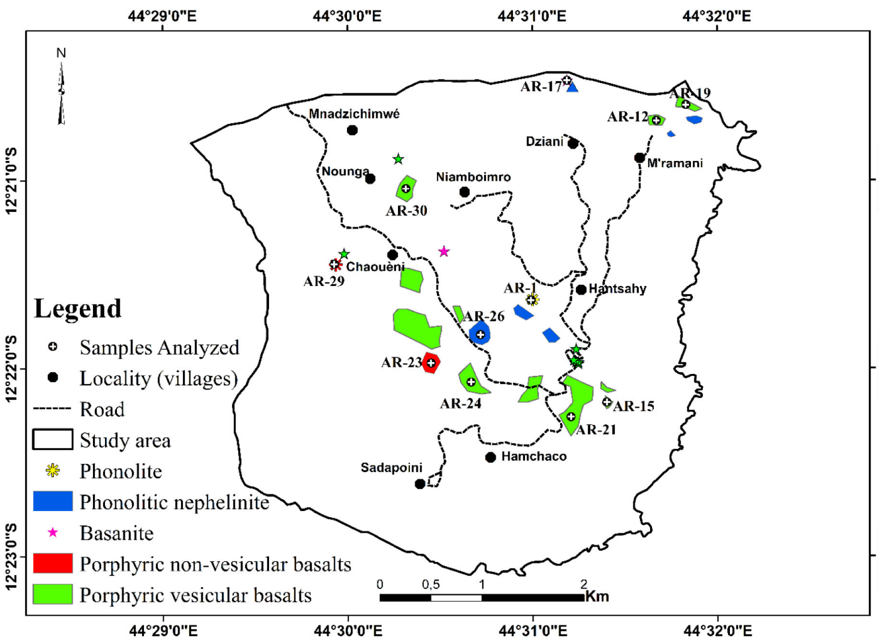

Figure 3. Outcrop map of the study area showing the locations of the samples analyzed.

Porphyric vesicular basalts constitute the most common facies in the study area. Based on the nature and distribution of the phenocrysts, these basalts can be are subdivided into three sub-facies: (i) vesicular basalts with olivine phenocrysts, (ii) vesicular basalts with olivine and clinopyroxene phenocrysts, and (iii) vesicular basalts with olivine, clinopyroxene and orthopyroxene phenocrysts. Vesicular basalts containing olivine phenocrysts crop out north-east of the study area, approximately 600 m from the village of Mramani, and to the south of the village of Hantsahy. Basalts bearing olivine and clinopyroxene phenocrysts are located south of the villages of Chaoueni and Hantsahy, north of Hamchaco, and north-east of Mramani. Finally, vésicular basalts with olivine, clinopyroxene and orthopyroxene phenocrysts occur approximately 100 m south of Chaoueni and about 250 m east and north-east of the village of Nounga. All these basalts display similar petrographic characteristics, with outcrops forming polygonal blocks, dark in color, and exhibiting elliptical vesicules of varying sizes (**Figure 4(a)**).

Under the microscope, the rocks show a porphyritic microlitic texture, with a primary minrealogical composition consisting of plagioclase, olivine, and pyroxene embedded in a relatively abundant mesostasis. Plagioalse (44% - 52%) occurs as abundant microlites. Olivine (13% - 20%) is present as both phenocrysts and microlites. Olivine phenocrysts (0.6 - 4.8 mm) are automorphic to subautomorphic, displaying vivid colors and cracking (**Figure 4(b)**). These phenocrysts are only rarely altered to iddingsite and opaque minerals. Pyroxenes (10% - 15%), represented by clinopyroxene and/or orthopyroxene, also occur as microlites and phenocrysts (**Figures 4(c)-(d)**), and are locally altered into opaque minerals. Opaque minerals (7% - 13%), generally xenomorphe in shape, result from the alteration of olivine and pyroxene.

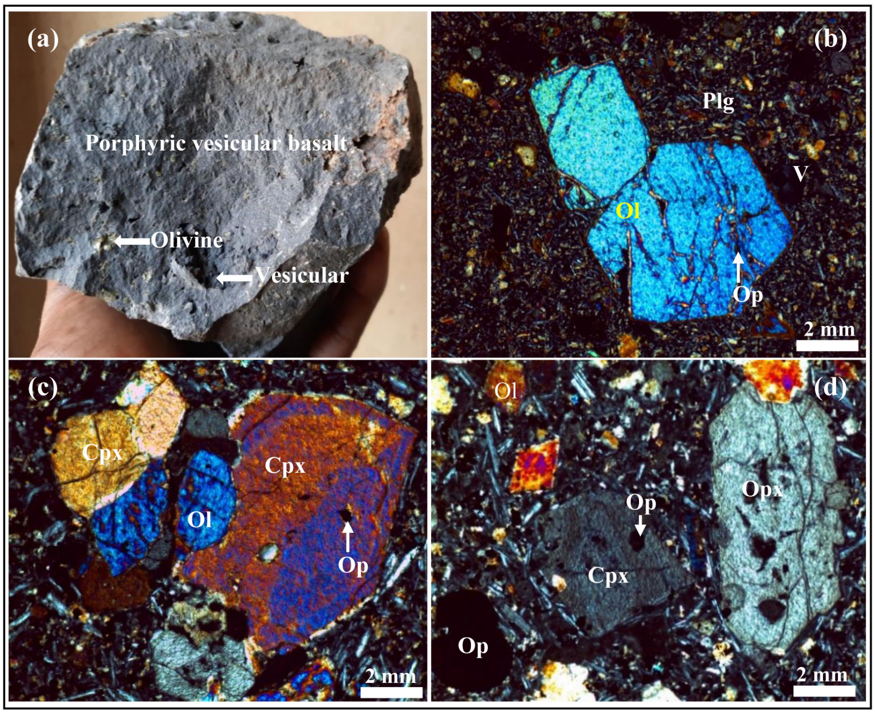

Figure 4. (**a**) (**b**) Macroscopic and microscopic characteristics of vesicular basalts (V) showing olivine (Ol) phenocrysts; (**c**) (**d**) microscopic characteristics of porphyritic vesicular basalts showing phenocrysts of olivine, clinopyroxene (Cpx), and orthopyroxene (Opx).

Porphyritic non-vesicular basalts are less frequent than their porphyritic vesicular basalts. They cropout to the south and west of the Chaoueni locality in the from of melanocratic polygonal blocks, cut by NNE - SSW-trending fractures (Figures 5(a)-(b)). Under the microscope, these rocks exhibit a porphyritic microlitic texture and a mineralogical composition characterized by a primary paragenesis of plagioclase, olivine and clinopyroxene, set within a relatively sparse mesostasis rich in opaque minerals (5% - 10%). Plagioclase (45% - 52%) occurs predominantly as microlites. Olivine (5% - 12%) and clinopyroxene (15% - 25%) occur both as microlites and as automorphic to subautomorphic phenocrysts, and are sometimes altered into xenomorphic opaque minerals. Clinopyroxene phenocrysts (0.8 - 6 mm) are occasionally twinned (Figure 5(c)) and may contain inclusions of olivine (Figure 5(d)). Olivine phenocrysts commonly display fractures, the margins of which are altered to iddingsite (Figure 5(e)).

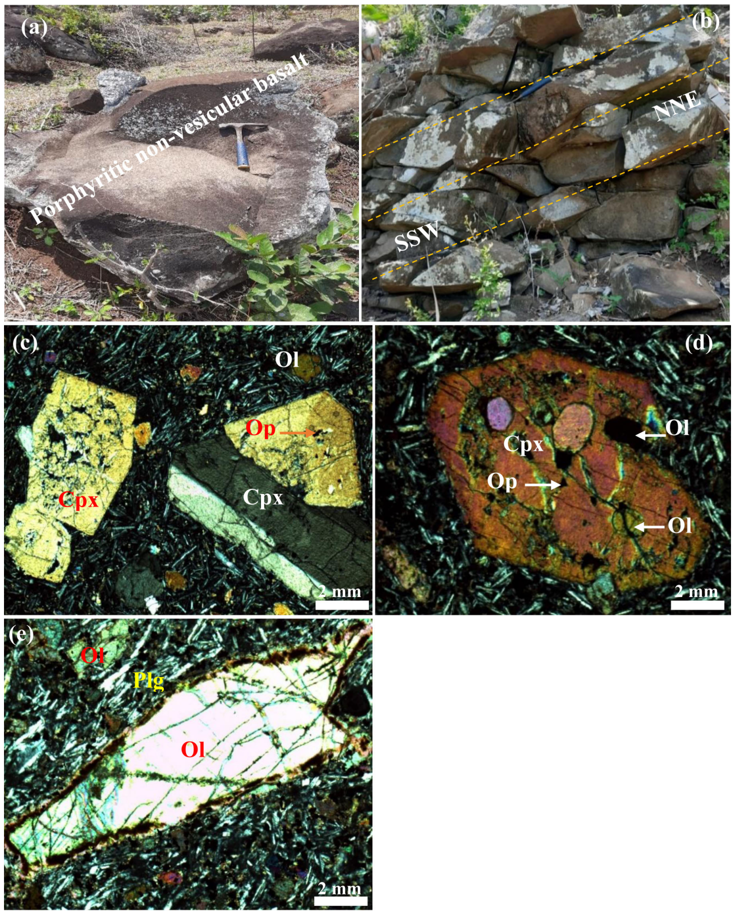

Figure 5. (a)-(e) Macroscopic and microscopic characteristics of non-vesicular basalts containing olivine (Ol) and clinopyroxene (Cpx) phenocrysts. The outcrops exhibits NNE-SSW-trending fractures (b). Olivine phenocrysts commonly show fracturing, with margins partially altered to opaque minerals (Op) and reddish iddingsite. Clinopyroxene phenocrysts enclose cracked olivine crystals and opaque minerals.

Basanites crop out approximately 100 m and north of the villages of Chaoueni and Dziani respectiveley, where they occur as small exposures composed of melanocratic polygonal blocks (Figure 6(a)). Petrographic observations reveal that these the basanites exhibit a porphyritic microlitic texture, with a primary mineral assemblage consisting of plagioclase, olivine, clinopyroxene and orthopyroxene set in a sparse mesostasis. In contrast to basalts, basanites are characterized by a lower abundance of plagioclase microlites (40% - 47%). Olivine (5% - 12%) typically occurs as both microcrystals and phenocrysts. Clinopyroxene (15% - 21%) commonly occurs as automorphic to subautomorphic phenocrysts (1.2 - 4.3 mm), but also as xenomorphic microcrystals. Clinopyroxene phenocrysts are frequently grouped into aggregates that include opaque minerals (Figure 6(c)). In contrast, orthopyroxene represents only about 5% of the rock volume and occurs predominantly as automorphic phenocrysts (1.9 to 2.8 mm) (Figure 6(b)). Opaque minerals (7% - 15%), occur in two forms: automorphic crystals enclosed within olivine, pyroxene, and plagioclase; and xenomorphic grains, resulting from the alteration of ferromagnesian minerals.

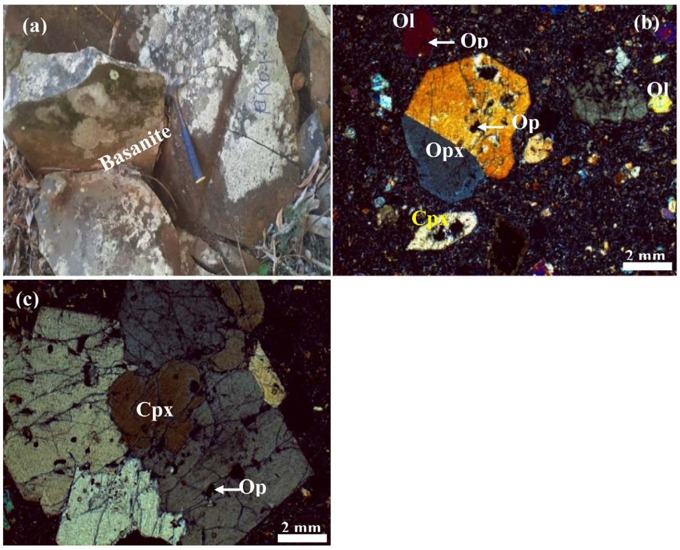

Figure 6. (**a**)-(**c**) Photographs and photomicrographs of basanite containing olivine (Ol), clinopyroxene (Cpx), and orthopyroxene (Opx). Orthopyroxene are twinned, whereas clinopyroxene occurs in aggregates.

Phonolitic nephelinites crop out at several locations, including approximately 350 m northeast of the village of Mramani, as well as to the west and north, and about 800 m north of the villages of Hantsahy, Dziani and Hamchaco, respectively. In outcrop, these rocks occur as polygonal blocks that are commonly rounded to subrounded. They are melanocratic in color and display small vesicules, generally elliptical in shape (Figure 7(a)). Under the microscope, the phonolitic nephelinites contain rare microphenocrysts of clinopyroxene (Figure 7(b)) and olivine embedded in a very abundant groundmass composed of plagioclase, olivine, clinopyroxene, and opaque mineral microlites. Clinopyroxene microphenocrysts (0.6 - 1.9 mm; 7% - 12%) are subautomorphic to automorphic, in shape and are occasionally altered to opaque minerals. Plagioclase microlites are highly abundant (45% - 50%). Olivine (2% - 5%) is less abundant and occurs mainly as microlites, and only rarely as microphenocrysts (0.3 - 0.8 mm), which are automorphic to subautomorphic, and may be partially altered into opaque minerals. Opaque minerals (25% - 33%) are very abundant and occur as xenomorphic microcrystals (0.3 - 0.6 mm).

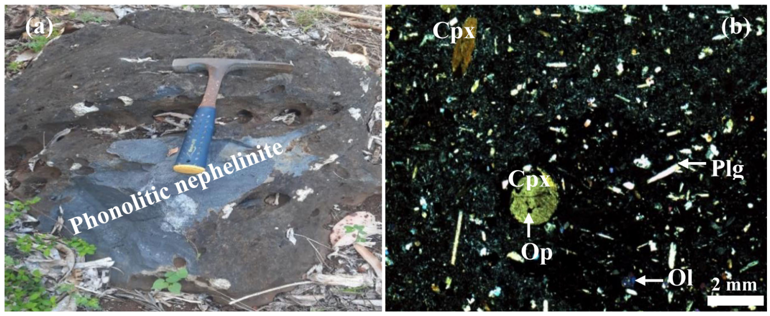

Figure 7. (a) (b) Macroscopic and microscopic characteristics of a phonolitic nephelinite showing rare clinopyroxene (Cpx) microphenocrysts within a very abundant groundmass rich in plagioclase (Plg), olivine (Ol), and opaque mineral (Op) microlites.

Phonolites are very rare and have limited spatial extent in our study area. They crop out exclusively to the west of the locality of Hantsahy, where they occur as polygonal blocks (Figure 8(a)). Under the microscopic, the rock reveals a fluidal microlitic texture, characterized by sanidine microlites (60% - 65%) oriented in the direction of lava flow (Figure 8(b)). The rock also contrain microlites and microphenocrysts (0.3 - 0.7 mm) of clinopyroxene (3% - 7%) and nepheline (2%), as well opaque minerals (17% - 25%) within a very abundant groundmass (Figures 8(b)-(c)).

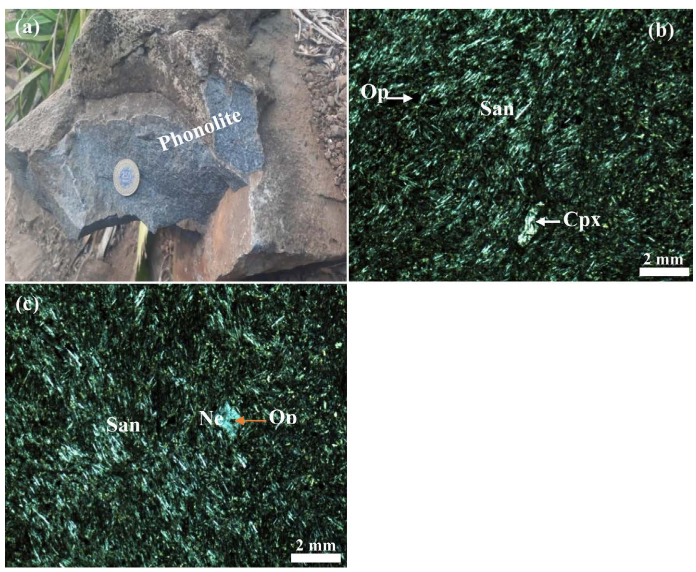

Figure 8. (a)-(c) Macroscopic and microscopic characteristics of a phonolite containing microphenocrysts of clinopyroxene and nepheline (Ne), displaying a fluidal texture marked by the preferred orientation of sanidine microlites (San) along the direction of lava flow.

4.2. Geochemistry

Eleven (11) rock samples corresponding to the fissural eruption phase were selected from the southern part of Anjoaun Island for geochemical analysis. The concentrations of major and trace elements, along with the lithological characteristics of these samples, are reported in Table 1 below. All samples display very low loss on ignition (LOI) values, ranging from - 0.2 to 1.4wt.%, suggesting minimal alteration during post-magmatic process such as low-grade metamorphism or water-rock interaction. Consequently, large ion lithophile elements (LILE) and high field strength elements (HFSE) are considered reliable for geochemical characterisation in the study. Rare earth element (REE) concentrations are normalized to NWA 974 chondrite values [33], whereas incompatible trace elements are normalized to the primitive mantle composition [34].

Table 1. Concentrations of major and trace elements in lava samples from the southern part of the Anjouan Island.

Lithology	**Alkaline basalt**								**Basanite**	**Nephelinite phonolitic**	**Phonolite**
Locality	Mramani		Hantsahy		Chaoueni		Hamchaco	Nounga	Dziani	Hamchaco	Hantsahy
Sample	AR-12	AR-19	AR-15	AR-21	AR-23	AR-29	AR-24	AR-30	AR-17	AR-26	AR-1
SiO_2	43.15	43.43	46.46	44.8	45.91	46.39	45.05	44.53	43.16	44.42	55.24
Al_2O_3	14.14	12.63	11.49	12.98	14.74	15.13	10.77	14.35	14.65	15.48	18.18
Fe_2O_3(T)	15.07	14.27	13.19	14.21	13.01	13.1	12.71	14.5	13.64	13.69	8.85
MnO	0.209	0.189	0.188	0.198	0.188	0.183	0.184	0.232	0.203	0.231	0.313
MgO	7.2	9.97	10.77	9.63	6.36	6.57	11.2	7.91	6.63	4.78	0.18
CaO	10.32	10.94	10.89	10.97	9.34	9.51	10.5	9.73	10.5	7.38	2.66
Na_2O	3.45	3.89	3.45	3.08	3.43	3.75	3.03	3.93	4.53	6.95	8.1
K2O	1.35	1.02	1.19	1.17	1.39	1.42	1.11	1.5	1.55	2.47	4.13
TiO_2	3.247	2.911	2.075	2.533	2.245	2.405	1.927	2.675	2.748	2.889	0.165
P_2O_5	0.66	0.69	0.53	0.66	0.7	0.6	0.48	0.65	0.85	0.88	0.12
LOI	-0.26	0.01	-0.16	0.43	1.41	0.39	0.98	0.2	-0.17	-0.25	1.3
Total	98.54	99.95	100.1	100.7	98.71	99.44	97.94	100.2	98.3	98.9	99.23
Mg#	64.26	72.44	75.44	71.83	64.78	65.36	76.98	67.24	64.65	56.78	7.12
Ni	110	260	320	190	110	110	340	140	110	30	< 20
Cr	200	520	870	460	210	180	950	260	160	< 20	< 20
Co	50	58	56	57	42	43	55	52	46	34	2
V	260	255	222	268	193	239	217	256	254	176	< 5
Cs	0.2	0.4	0.3	0.3	0.3	0.4	0.2	0.5	0.5	0.6	1.1
Rb	24	25	31	27	33	35	28	40	36	64	108
Ba	575	532	444	675	515	494	562	689	595	1100	1426

Continued

Th	3.33	5.26	4.79	3.58	6.08	5.27	4.21	5.61	6.31	19.2	13.8
U	0.68	1.16	1.2	0.74	1.68	1.29	0.8	1.27	1.68	4.4	2.7
Nb	46.2	50.7	43.3	41.5	50.2	45.3	38.4	51.9	63.1	102	111
La	37	46.1	40.9	40.2	50.7	40.6	36.8	49.5	54	103	117
Ce	74.3	91.1	79.5	75.4	96.7	77.9	71.5	92.9	108	182	197
Pb	<5	<5	5	<5	5	<5	<5	5	6	15	15
Pr	9.05	10.8	9.2	9.1	11	9.18	8.38	10.8	12.6	19.2	20.6
Sr	871	791	620	664	754	684	647	900	905	1412	922
Nd	37.9	43.5	35.9	36.1	42.3	34.8	33.6	41.9	49	68.8	70.5
Zr	138	194	198	149	223	203	187	194	239	281	464
Sm	8.36	9.01	7.44	7.58	8.53	7.52	6.99	8.52	9.93	12.7	11.9
Eu	2.7	2.89	2.41	2.49	2.72	2.32	2.15	2.64	3.26	3.92	3.41
Gd	7.43	7.69	6.61	6.87	7.08	6.43	5.84	7.24	8.35	10.1	9.1
Dy	6.06	5.89	4.97	5.52	5.87	5.28	4.72	5.99	6.59	8.06	8.06
Ho	1.02	0.99	0.86	0.97	1.07	0.98	0.81	1.07	1.1	1.44	1.54
Er	2.8	2.41	2.3	2.58	2.59	2.54	2.09	2.83	2.95	3.83	4.37
Y	27.8	24.4	22.8	26.2	26.9	25.4	21.1	26.6	29.8	38.9	44
Yb	2.07	1.72	1.69	2.04	2.04	2.06	1.57	2.2	2.24	3.32	4.03
Lu	0.303	0.239	0.252	0.312	0.302	0.298	0.238	0.326	0.333	0.503	0.61
Sn	1	2	1	1	2	2	1	1	2	2	3
Sb	< 0.2	< 0.2	< 0.2	< 0.2	< 0.2	< 0.2	< 0.2	0.2	< 0.2	0.3	0.2
Tb	1.12	1.12	0.96	1	1.09	1.01	0.88	1.1	1.26	1.48	1.43
W	< 0.5	0.8	0.5	< 0.5	0.6	0.6	< 0.5	1	1	3	1.2
Ta	2.45	2.98	2.57	2.33	2.99	2.84	2.33	2.95	4.09	5.42	6.68
Mo	< 2	2	2	< 2	2	2	< 2	3	3	8	3
Hf	3.7	4.6	4.6	3.6	5.1	4.8	4.2	4.4	5.1	5.7	8.7
ΣREE (ppm)	1078.21	1228.42	1059.68	1065.57	1263.21	1061.03	967.19	1247.26	1418.90	2200.26	2343.14
La_N/Yb_N	16.86	25.28	22.82	18.58	23.44	18.59	22.10	21.22	22.73	29.26	27.38
La_N/Sm_N	3.16	3.66	3.93	3.79	4.25	3.86	3.76	4.15	3.89	5.80	7.03
Gd_N/Yb_N	3.43	4.27	3.74	3.22	3.31	2.98	3.55	3.14	3.56	2.91	2.16
Eu/Eu*	0.90	0.91	0.91	0.91	0.92	0.88	0.88	0.88	0.94	0.90	0.85

4.2.1. Classification and Magmatic Affinity

Plotting the samples from the southern part of Anjouan Island on the total alkali-silica ($Na_2O + K_2O$ vs. SiO_2) classification diagram [35] (**Figure 9**) indicates that the lavas comprise alkali basalts, basanite-tephrites, phonolitic nephelinites, and phonolites, all of which fall within the field of silica-undersaturated alkaline rocks. However, the sample falling within the basanite-tephrite field is classified as a basanite, owing to its olivine content exceeding 10% [36].

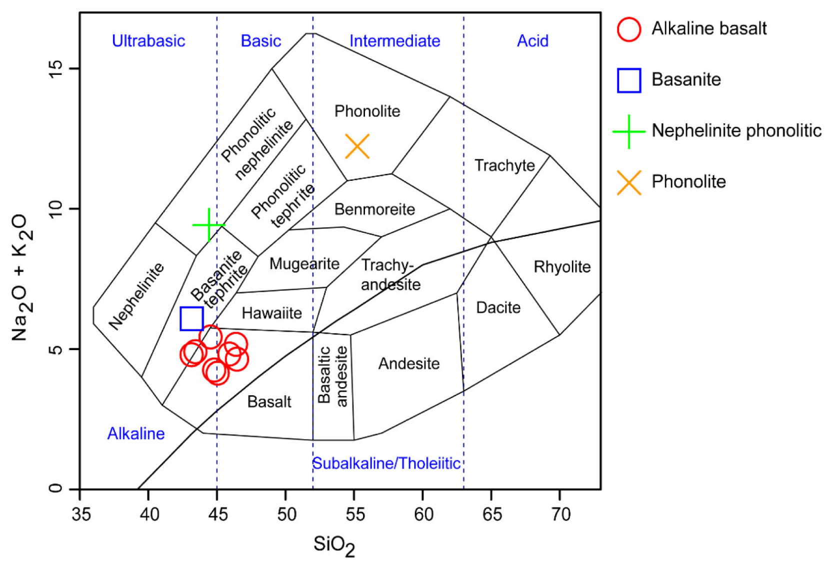

Figure 9. Total alkali-silica ($Na_2O + K_2O$ vs. SiO_2) diagram [35] showing the classification and magmatic affinity of lavas from the southern part of Anjouan island.

4.2.2. Major and Trace Elements

Alkaline basalts are characterized by SiO_2 contents ranging from 43.1 to 46.5 wt.%, TiO_2 1.9 to 3.2 wt.%, Al_2O_3 from 10.8 to 15.1 wt.%, MgO from 6.36 to 11.2wt.%, FeO(t) from 12.7 and 15.1wt.%, CaO from 9.3 and 11 wt.%, Na_2O from 3 and 3.9 wt.%, MnO at 0.2 wt.%, K_2O from 1.0 and 1.5 wt.%, P_2O_5 from 0.5 to 0.7 wt.% (**Figure 10**). The Mg number (Mg# = [MgO/40.3/(MgO/40.3 + FeO/71.85)] * 100) ranges from 64.3 to 77. Compatible trace elements concentrations show that Ni ranges 110 to 340 ppm, Cr from 120 to 950 ppm, Co from 42 to 52 ppm and V from 193 to 268 ppm. The relatively high contents of MgO, FeO(t), Ni and Co are consistent with olivine fractionation. Similarly, the concentrations of CaO, Cr, and V suggest the involvement of clinopyroxene crystallization of clinopyroxene crystallization, whereas the elevated Al_2O_3, Na_2O and CaO contents are indicative of plagioclase crystallization.

Alkaline basalts (ΣREE = 967 - 1 263 ppm) are characterized by steeply sloping rare earth element (REE) patterns (La_N/Yb_N = 16.9 - 25.3), marked by strong enrichment in light REE (LREE), ranging from 233 to 321 times chondritic values, and depletion in heavy REE (HREE), ranging from 10 to 14 times chondritic values. These patterns are accompanied by very slight negative europium anomalies (Eu/Eu* = 0.88 - 0.91) (**Figure 11(a)**). On the primitive mantle-normalized multi-élément diagram (**Figure 11(b)**), the alkaline basalts display positive anomalies in Ba, Nb, and Sr, and negative anomalies in Th, U, Pr, Zr, and Yb. An exception is represented by samples AR-23, which exhibits negative Nb and Sr anomalies and a positive anomaly U anomaly.

Basanite exhibits geochimical characteristics very similar to those of alkali basalts, except for its higher Na_2O (4.5 wt.% compared 3.0 - 3.9 wt.%) and P_2O_5 (0.8

wt.% compared to 0.5 - 0.7 wt.%) contents (**Figure 10**). It is also generally enriched in rare earth elements (ΣREE = 1419 ppm) and displays a less pronounced negative europium anomaly (Eu/Eu* = 0.94, versus 0.88 - 0.91 in alkali basalts) (**Figure 11(a)**). On the primitive mantle-normalized multi-element diagram (**Figure 11(b)**), the basanite exhibits patterns of positive and negative anomalies to those observed in the alkali basalts, except for uranium, which display a positive anomaly.

Phonolitic nephelinite differs from alkali basalts and basanite by its higher Na_2O (6.9 wt.% compared to 3.0 - 3.9 wt.% and 4.5 wt.% respectively) and K_2O contents (2.5 wt.% compared 1.0 - 1.5 wt.% and 1.55 wt.%). In contrast, it exhibits lower MgO (4.8 wt.% compared to 6.4 - 11.2 wt.% and 6.6 wt.%), CaO (7.4 wt.% compared 9.3 - 11 wt.% and 10.5 wt.%) (**Figure 10**), and Mg # (56.8 compared to 64.3 - 77 and 64.6). It is also strongly enriched in light rare earth elements (LREE), reaching up to 652 times chondritic values, and in heavy rare earth elements (HREE), up to 21 times chondritic values, with a more fractionated REE pattern (La_N/Yb_N = 29.3 versus to 16.9 - 25.3 for alkali basalts and 22.7 for basanite) (**Figure 11(a)**). On the primitive mantle-normalized multi-element diagram (**Figure 11(b)**), the phonolitic nephelinite displays patterns of positive and negative anomalies to those of the alkali basalts, except for positive anomalies in Th and U a negative anomaly in Nb.

Finally, phonolite is clearly distinguished from the other lava types by its higher Al_2O_3 (18.18 wt.%), Na_2O (8.1 wt.%), MnO (0.3 wt.%), and K_2O (4.1 wt.%), contents, as well as its lower concentrations of TiO_2, (0.2 wt.%), MgO (0.2 wt.%), FeO(t) (8.8 wt.%), CaO (2.7 wt.%), P_2O_5 (0.12 wt.%) (**Figure 10**), together with a very low Mg # (7.1). It is also strongly enriched in rare earth elements (ΣREE = 2343 ppm), with LREE concentrations reaching up to 740 times chondritic values and HREE concentrations up to 25 times chondritic values. The REE pattern is characterized by a more pronounced negative europium anomaly (Eu/Eu* = 0.85) (**Figure 11(a)**). The phonolite is further distinguished by a negative Sr anomaly and a positive Zr anomaly on the primitive mantle-normalized multi-element diagram (**Figure 11(b)**). These geochemical features, together with the very low MgO content, indicate a magma that has undergone extensive fractionation of olivine, plagioclase, and pyroxene.

In summary, the geochemical characteristics of the lavas from the southern part of the Anjouan island suggest a genetic relationship and a progressive magmatic evolution from alkali basalts to phonolites, through basanites and phonolitic nephelinites. This differentiation trend, driven by fractional crystallization, is reflected in a gradual decrease in TiO_2, MgO, FeO(t), CaO, Ni and Cr, contents, accompanied by a concomitant increase in SiO_2, Al_2O_3, Na_2O, MnO and K_2O (**Figure 10**). This evolutionary process is further evidenced by the continuous enrichment and sub-parallelism of REE patterns, from the least evolved rocks (alkali basalts) to the most evolved ones (phonolites), passing successively through basanites and phonolitic nephelinites (**Figure 11(a)**). Finally, it should be noted that all the lava types display positive Nb anomalies, with the exception of the alkali basalt sample AR-23 and the phonolitic nephelinite sample (AR-26) (**Figure 11(b)**).

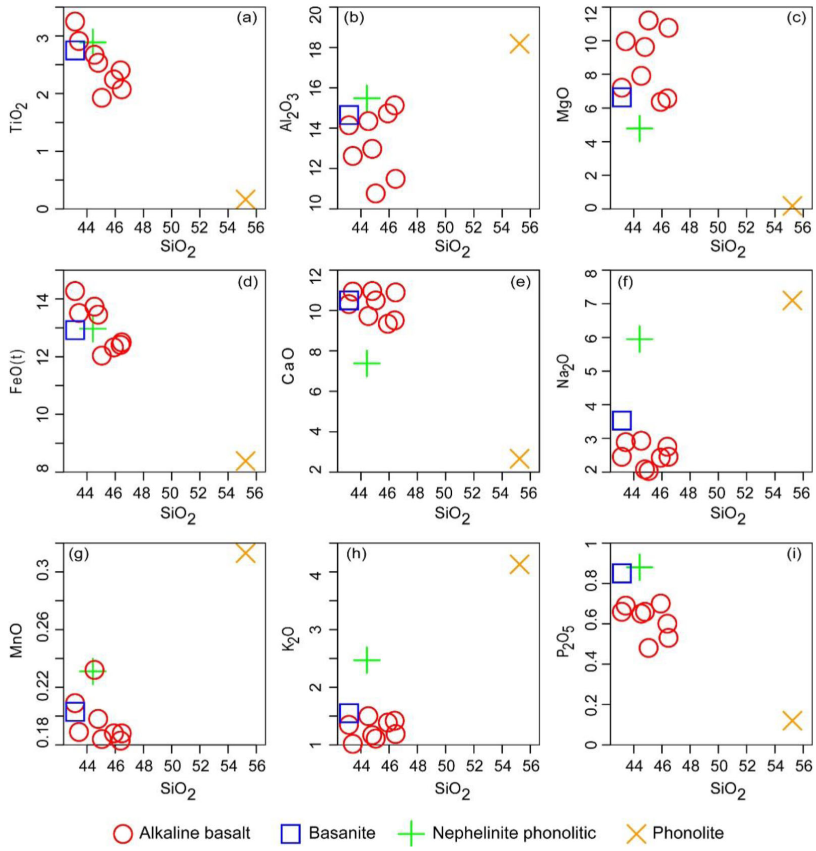

Figure 10. Harker diagrams illustrating the variation of major oxide compositions as a function of SiO_2 in lavas from the southern part of Anjouan island.

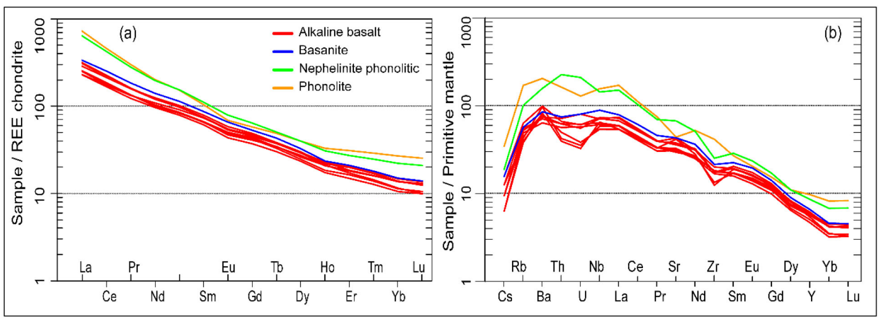

Figure 11. Diagrams illustrating: **(a)** REE spectra normalized to NWA974 chondrite values [33], and **(b)** primitive mantle-normalized multi-element patterns of incompatible trace elements in lavas from the southern part of Anjouan Island [34].

4.2.3. Nature and Depth of the Magmatic Source

To constrain the nature of the magma source, only the mafic lavas (alkali basalts and basanites), which are representative of primary magmatic liquids, were plotted on the Sm/Yb (ppm) versus La/Yb (ppm) diagram [36] (**Figure 12(a)**). On this diagram, both the alkali basalts and basanite plot within the enriched mantle field and show a close correlation with melting curves of asthenospheric mantle in the garnet lherzolite facies. The same samples were also plotted on the TiO_2/Yb (ppm) versus Nb/Yb (ppm) diagram from [37] (**Figure 12(b)**), which was developed to estimate the depth of magma sources in oceanic settings unaffected by subduction. This diagram confirms the alkaline nature of the lavas and places them within the garnet stability field, suggesting a deep mantle source of garnet lherzolite composition. The presence of garnet in the source is further supported by the markedly depleted heavy rare earth element (HREE) patterns, which reflect the retention of HREE by residual garnet. In addition, previous studies [38]-[40] have shown that high Ba/Rb ratios associated with low Rb/Sr ratios indicate an amphibole-bearing source, whereas low Ba/Rb ratios suggest the presence of phlogopite. Accordingly, the relatively high Ba/Rb ratios (14.11 - 25) and low Rb/Sr ratios (0.02 - 0.05) observed in the studied mafic lavas are consistent with a magma derived from a source in equilibrium with amphibole-bearing mantle.

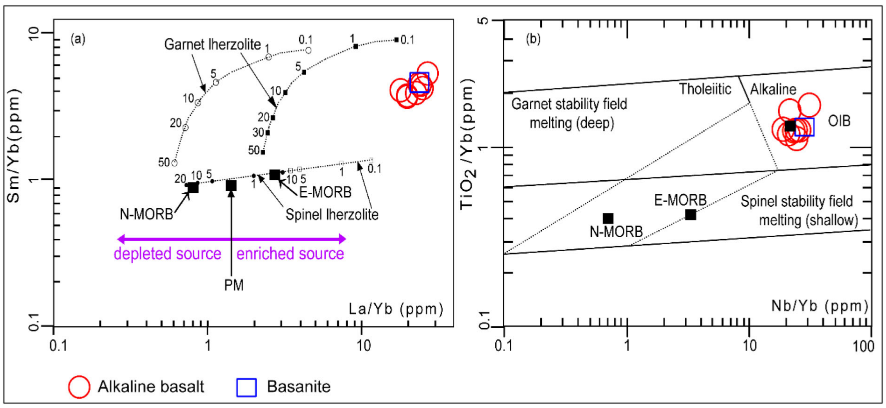

Figure 12. Diagrams: **(a)** Sm/Yb (ppm) vs La/Yb (ppm) [36] and **(b)** TiO2/Yb (ppm) vs Nb/Yb (ppm) [37], showing the nature and depth of the source lavas in the southern part of Anjouan Island. PM = Primitive Mantle; N-MORB = Normal Mid-Ocean Ridge Basalt; E-MORB = Enriched Mid-Ocean Ridge Basalt; OIB = Ocean Island Basalt. Data from [34].

4.2.4. Geodynamic Context

To constrain the geodynamic setting of the lavas from the southern part of Anjouan Island, triangular and binary diagrams involving elements considered immobile or relatively immobile during alteration and metamorphic processes were employed. Accordingly, the Th - Zr/117 - Nb/16 [41] (**Figure 13(a)**) and Zr/4 - 2Nb - Y [42] (**Figure 13(b)**) plot all the lavas from the southern part of Anjouan Island within the field of intraplaque basalts (WPA or AI). These results are further supported by the FeO(t) - MgO - Al_2O_3 diagram [43] (**Figure 13(c)**), the Ti (ppm) versus V (ppm) [44] (**Figure 13(d)**), Nb/Y versus Zr/Y [45] (**Figure 13(e)**), and Th/Yb versus Nb/Yb [37] (**Figure 13(f)**), all of which place the samples within the domain of alkaline basalts and/or ocean island basalts (OIB-AB or OIB). It should be noted, however, that this geodynamic setting is consistent with the strongly LREE-enriched patterns and the positive Nb anomalies observed in the samples (except for sample AR-23). It also consistent with the position of all the lavas from the southern part of Anjouan Island above the ΔNb line on the Nb/Y versus Zr/Y diagram [45] (**Figure 13(e)**), indicating that their source is related to a mantle plume originating from an enriched lower mantle. The magma is inferred to have ascended through a hotspot activity mecanism, facilitated by lithospheric fractures.

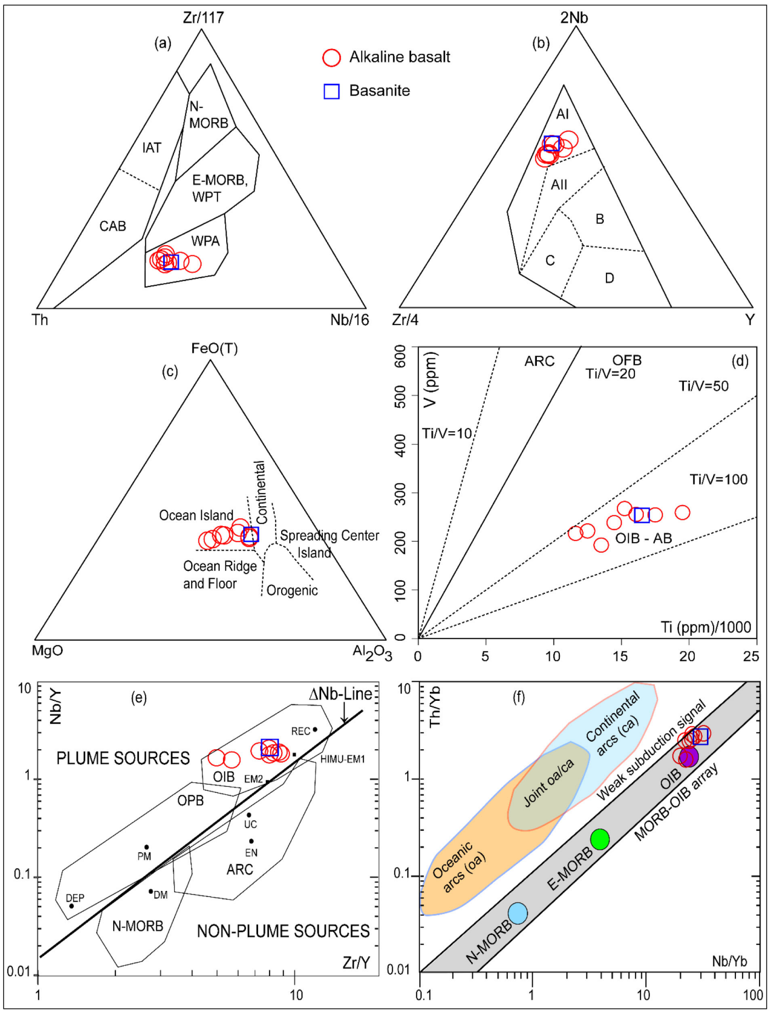

N-MORB = Normal Mid-Ocean Ridge Basalts; E-MORB = Enriched Mid-Ocean Ridge Basalts; IAT = Island Arc Tholeiites; CAB = Volcanic Arc Basalts; WPT = Tholeiitic Within-Plate basalts; WPA = Alkaline Within-Plate basalts; AI = Within-plate alkali basalt; AII = Within-plate alkali basalt and within-plate tholeiites; B = E-MORB; C = Within-plate tholeiites and volcanic arc basalts; D = N-MORB and volcanic arc basalts; ARC = arc related basalts; OFB = Ocean Flood Basalts; OIB-AB = Ocean Island Basalts and Alkali Basalt; OPB = Oceanic Plateau Basalts. Hypothetical mantle sources: DM = shallow depleted mantle; EN = enriched component; PM = primitive mantle; REC = recycling component; UC = upper continental crust; DEP = depleted plume component; HIMU = high (U/Pb) source; EM1 and EM2 = enriched mantle sources (modified after [45] [46]).

Figure 13. Diagrams: (a) Th - Zr/117 - Nb/16 [41], (b) Zr/4 - 2Nb - Y [42], (c) FeO(t) - MgO - Al_2O_3 [43], (d) Ti (ppm) vs V (ppm) [44], (e) Nb/Y vs Zr/Y [45] and (f) Th/Yb vs Nb/Yb [37] showing the composition ranges of various oceanic lavas, within which the lavas from the southern part of Anjouan Island are plotted.

5. Discussion

The southern part of Anjouan Island is characterized by a diverse assemblage of volcanic rocks, including alkaline basalts, basanites, phonolitic nephelinites, and phonolites. At the outcrop scale, these rocks occur in both vesicular and non-vesicular facies and display porphyritic textures as well as fluidal microlitic textures. Their mineralogical composition reflects a sequential crystallization of opaque minerals, followed, by olivine, clinopyroxene, orthopyroxene, plagioclase, sanidine, and nepheline. This sequence is consistent with those reported for alkaline lavas from Grande Comore ([15] [47] [48]), Réunion Island ([49] [50]), Hawaii ([51] [52]), and Iceland ([53]). However, it is noteworthy that orthopyroxene, nepheline, and sanidine have not been documented in some alkaline lava series from Grande Comore ([15] [47]) and Réunion ([49]). In contrast, the crystallization sequence identified in the Anjouan lavas differs from that reported for alkaline lavas from Possession Island (Crozet Archipelago) [54], where opaque minerals crystallize at a later stage. It also contrasts with the sequence described for Karthala lavas (Grande Comore) [55], in which olivine crystallizes prior to opaque minerals.

The geochemical data indicate the alkaline nature and silica undersaturation of the magma, as well as enrichment in light rare earth elements (LREE) and depletion in heavy rare earth elements (HREE), reflected in strongly fractionated patterns and the presence of positive Nb anomalies in the lavas from the southern part of Anjouan Island. These geochemical characteristics are consistent with derivation from a highly enriched, deep-seated garnet-bearing lherzolitic source located within the lower mantle, which is inferred to have ascended as a mantle plume and generated hotspot-related magmatism. These findings are in agreement with studies conducted on Anjouan Island and other islands of the Comoros Archipelago (Mayotte, Mohéli, and Grande Comore) ([3] [4] [48] [56]-[60]). Moreover, the high Mg# values (64.3 - 77) and relatively low SiO_2 contents (43.15 - 46.46 wt.%) of the alkaline basalts from the southern part of Anjouan island suggest a primary or near-primary magma composition. The primary nature of magmas within the Comoros Archipelago has previously been reported for the alkaline basalts of La Grille, in contrast to the more evolved, non-primary alkaline lavas of Karthala, which are characterized by lower Mg# values (0.52 - 0.54) [56]. Furthermore, the lavas of the archipelago display a compositional evolution from south to north, with more evolved compositions (ranging from alkaline basalts to phonolites) occurring in the southern islands, such as Mayotte ([12] [59]), and Anjouan, whereas the northern island of Grande Comore is dominated by less evolved lithologies, including alkaline basalts, pahoehoe and "aa" lava flows, ankaramites, and oceanites [48].

Furthermore, it should be noted that the lavas of the Comoros Archipelago display significant geochemical variability. This variability has been interpreted by several authors as resulting from: (i) variations in the degree of partial melting, (ii) differences in the depth of melting, (iii) the involvement of a metasomatized mantle source, and/or (iv) recycling processes. With regard to degree and depth of partial melting, the lavas from the southern part of Anjouan Island, characterized by high LREE/HREE ratios, are interpreted as the products of low-degree partial melting of a deep garnet-bearing lherzolitic source. In addition, the involvement of hydrated phase, such as amphibole, in the mantle source is suggested by relatively high Ba/Rb ratios (14.11 - 25) coupled with low Rb/Sr ratios (0.02 - 0.05) ([38]-[40]). The presence of an amphibole-bearing source has previously been proposed for lavas from La Grille ([4] [56] [58]), Mayotte [49], Mohéli [60], and Karthala ([15] [48] [57]). In contrast, these results differ from those reported for lavas from Karthala ([4] [56]) and Mohéli [56], which are interpreted as having been generated from a relatively higher degree of partial melting of a garnet-or spinel-bearing lherzolitic source at shallower depths. Finally, some authors have proposed that the lavas of La Grille [58], Mayotte [59], and Mohéli [60] derive from a mantle source metasomatized by CO_2-rich fluids, in the presence of mineral phases such as apatite, dolomite, or phlogopite. In contrast, other studies ([47] [48]) suggest that the Karthala lavas reflect recycling processes within the mantle plume, involving contributions from residues of the oceanic lithosphere.

6. Conclusions

The southern part of the island of Anjouan, located in the Comoros archipelago, is characterized by a diverse assemblage of volcanic rocks, including alkaline basalts, basanites, phonolitic nephelinites, and phonolites. These rocks, which occur as both vesicular and non-vesicular facies, exhibit porphyritic and fluidal textures and are defined by a mineralogical composition reflecting the crystallization of opaque minerals, olivine, clinopyroxene, orthopyroxene, plagioclase, sanidine, and nepheline.

The geochemical study highlights the primary nature of an alkaline, silica-undersaturated magma that evolved from alkaline basalts to phonolites, through basanites and phonolitic nephelinites, respectively. The geochemical data also indicate enrichment in light rare earth elements (LREE) and depletion in heavy rare earth elements (HREE), reflected by strongly fractionated patterns and the presence of positive Nb anomalies. These geochemical features are typical of alkaline basaltic magmas generated by a low degree of partial melting of a highly enriched, deep-seated garnet-bearing lherzolitic source containing amphibole, located within the lower mantle. A mantle plume is inferred to have originated from this source, leading to magma emplacement in an oceanic intraplate setting associated with hotspot activity through lithospheric fractures. However, several hypotheses have been proposed to explain the compositional diversity of lavas within the Comoros Archipelago, including variations in the degree and depth of partial melting, the involvement of a mantle source metasomatized by CO_2-rich fluids, and recycling processes involving the oceanic lithosphere. In the context, isotopic geochemistry would provide a valuable complement for better constraining the processes of recycling and potential contamination.

Acknowledgments

We would like to express our sincere gratitude to all those who contributed to the preparation of this article. Special thanks are extended to Mr. Baba SAAR and Ms. Safiétou Senghor THIAM of the Petrology and Structural Geology Laboratory at the Fundamental Institute of Black Africa (IFAN) of Cheikh Anta Diop University of Dakar (UCAD), Senegal for the warm and support during the microscopic observation sessions. Finally, we would like to express our deep appreciation to the parents of Mr. Ali Rachidi OIKIFOU, whose unwavering support and personal dedication made this work possible. This article is dedicated to them in recognition of the values and principles they instilled in him.

Conflicts of Interest

The authors declare no conflicts of interest regarding the publication of this paper.

References

[1] Ludden, J.N. (1977) The Mineral Chemistry and Origin of Xenoliths from the Lavas of Anjouan, Comores Archipelago, Western Indian Ocean. *Contributions to Mineralogy and Petrology*, **64**, 91-107. https://doi.org/10.1007/bf00375287

[2] Maugé, L.A., Ségoufin, J., Vernier, E. and Froget, C. (1982) Geomorphologie et Origine des Bancs du Nord-Est du Canal de Mozambique—Ocean Indien Occidental (Geomorphology and Origin of the Reef-Banks of the North-Eastern Mozambique Channel—Western Indian Ocean). *Marine Geology*, **47**, 37-55. https://doi.org/10.1016/0025-3227(82)90018-4

[3] Quidelleur, X., Michon, L., Famin, V., Geffray, M., Danišík, M., Gardiner, N., *et al*. (2022) Holocene Volcanic Activity in Anjouan Island (Comoros Archipelago) Revealed by New Cassignol-Gillot Groundmass K-Ar and ^{14}C Ages. *Quaternary Geochronology*, **67**, Article ID: 101236. https://doi.org/10.1016/j.quageo.2021.101236

[4] Deniel, C. (1998) Geochemical and Isotopic (Sr, Nd, Pb) Evidence for Plume-Lithosphere Interactions in the Genesis of Grande Comore Magmas (Indian Ocean). *Chemical Geology*, **144**, 281-303. https://doi.org/10.1016/s0009-2541(97)00139-3

[5] Dofal, A. (2021) Structure de la lithosphère de l'océan Indien occidental révélée par la méthode des fonctions réceptrices. Thèse de doctorat, Université de La Réunion, 344 p.

[6] Mirhani, N. (2014) Dynamique d'évolution des géosystèmes en milieu tropical humide insulaire: Approche par les bassins versants d'Anjouan aux Comores. Ph.D. Thesis, De l'Université d'Angers et de l'Université de Toliara, 255 p.

[7] De Saint Ours, J. (1960) Etudes géologiques dans l'extrême nord de Madagascar et l'archipel des Comores. Rapport Service géologique de Tananarive, 205 p.

[8] Lacroix, A. (1922) La constitution lithologique de l'archipel des Comores. *Comptes Rendus du XIIIème Congrès Géologique International*, Bruxelle, 10 au 19 août 1922, 949-979.

[9] Flower, M.F.J. and Strong, D.F. (1969) The Significance of Sandstone Inclusions in Lavas of the Comores Archipelago. *Earth and Planetary Science Letters*, **7**, 47-50. https://doi.org/10.1016/0012-821x(69)90010-7

[10] Esson, J., Flower, M.F.J., Strong, D.F., Upton, B.G.J. and Wadsworth, W.J. (1970) Geology of the Comores Archipelago, Western Indian Ocean. *Geological Magazine*, **107**,

549-557. https://doi.org/10.1017/s0016756800058647

[11] Montaggioni, L.F. and Nougier, J. (1981) Les enclaves de roches detritiques dans les Volcans d'Anjouan (Archipel des Comores); Origine et interpretation dans le cadre de l'evolution du Canal de Mozambique. *Bulletin de la Société Géologique de France*, **7**, 595-601. https://doi.org/10.2113/gssgfbull.s7-xxiii.6.595

[12] Debeuf D. (2004) Etude de l'évolution volcano-structurale et magmatique de Mayotte (Archipel des Comores, Océan Indien). Approches structurale, pétrographique, géochimique et géochronologique. Thèse de doctorat, Université de La Réunion, 277 p.

[13] Wright, J.B. and McCurry, P. (1970) The Significance of Sandstone Inclusions in Lavas of the Comores Archipalago, M.F.J. Flower and D.F. Strong. *Earth and Planetary Science Letters*, **8**, 267-268. https://doi.org/10.1016/0012-821x(70)90188-3

[14] Rabinowitz, P.D., Coffin, M.F. and Falvey, D. (1983) The Separation of Madagascar and Africa. *Science*, **220**, 67-69. https://doi.org/10.1126/science.220.4592.67

[15] Desgrolard, F. (1996) Pétrologie des laves d'un volcan intraplaque océanique: Le Karthala, île de la Grande Comore (R.F.I des Comores). Thèse de doctorat, Université Blaise-Pascal, 176 p.

[16] Savin, C. (2001) Circulation hydrothermale au sein du volcan Karthala (île de la Grande Comore-Océan Indien): Apports de la géophysique. Thèse de Doctorat, Université de La Réunion, 308 p.

[17] Masquelet, C. (2023) Magmatisme, héritage et déformation autour de l'archipel des Comores, dans le bassin de Somalie: Implications géodynamiques. Thèse de doctorat, Sorbonne Université, 201 p.

[18] Roche, V. and Ringenbach, J. (2022) The Davie Fracture Zone: A Recorder of Continents Drifts and Kinematic Changes. *Tectonophysics*, **823**, 229188. https://doi.org/10.1016/j.tecto.2021.229188

[19] Talwani, M. (1962) Gravity Measurements on HMS Acheron in South Atlantic and Indian Oceans. *Geological Society of America Bulletin*, **73**, 1171-1182. https://doi.org/10.1130/0016-7606(1962)73[1171:gmohai]2.0.co;2

[20] Hajash, A. and Armstrong, R.L. (1972) Paleomagnetic and Radiometric Evidence for the Age of the Comores Islands, West Central Indian Ocean. *Earth and Planetary Science Letters*, **16**, 231-236. https://doi.org/10.1016/0012-821x(72)90195-1

[21] Emerick, C.M. and Duncan, R.A. (1982) Age Progressive Volcanism in the Comores Archipelago, Western Indian Ocean and Implications for Somali Plate Tectonics. *Earth and Planetary Science Letters*, **60**, 415-428. https://doi.org/10.1016/0012-821x(82)90077-2

[22] Bachèlery, P., Berthod, C., Di Muro, A., Gurioli, L., Besson, P., Caron, B., *et al.* (2019) Petrological and Geochemical Characterization of the Lava from the 2018-2019 Mayotte Eruption: First Results. *American Geophysical Union*, *Fall Meeting* 2019, San Francisco.

[23] Bachèlery, P., Morin, J., Villeneuve, Soulé, H., Nassor, H. and Ali, A.R. (2015) Structure and Eruptive History of Karthala Volcano. In: Bachelery, P., Lenat, J.F., Di Muro, A. and Michon, L., Eds., *Active Volcanoes of the Southwest Indian Ocean*, Springer, 345-366.

[24] Upton, B.G.J. (1982) Oceanic Islands. In: Nairn, A.E.M. and Stehli, F.G., Eds., *The Ocean Basins and Margins*, Springer, 585-648. https://doi.org/10.1007/978-1-4615-8038-6_13

[25] Obura, D.O., Burgener, V., Nicoll, M.E., Ralison, H.O. and Scheren, P. (2015) The

Northern Mozambique Channel. Setting the Foundations for a Regional Approach to Marine Governance. A Background Document. WWF International and CORDIO East Africa.

[26] Mougenot, D., Raillard, S. and Virlogeux, P. (1987) Structure de la marge et du canal de Mozambique. *Actes du Colloque sur la Recherches Francaise dans les Terres Australes*, Strasbourg, 14-17 Septembre 1987, 323-336.

[27] Malod, J.A., Mougenot, D., Raillard, S. and Maillard, A. (1991) Nouvelles contraintes sur la cinématique de Madagascar: Les structures de la chaîne de Davie. *Comptes rendus de l'Académie des Sciences*, **312**, 211-214.

[28] Dofal, A., Fontaine, F.R., Michon, L., Barruol, G. and Tkalčić, H. (2021) Nature of the Crust Beneath the Islands of the Mozambique Channel: Constraints from Receiver Functions. *Journal of African Earth Sciences*, **184**, Article ID: 104379. https://doi.org/10.1016/j.jafrearsci.2021.104379

[29] Flower, M.F.J. (1972) Petrology of Volcanic Rocks from Anjouan, Comores Archipelago. *Bulletin Volcanologique*, **36**, 238-250. https://doi.org/10.1007/bf02596993

[30] De Saint Ours, J. and Pavlovsky, R. (1952) Etude géologique de l'Archipel des Comores. Haut-de Madagascar et de ses Dépendances.

[31] Thompson, R.N. and Flower, M.F.J. (1971) One-Atmosphere Melting and Crystallization Relations of Lavas from Anjouan, Comores Archipelago, Western Indian Ocean. *Earth and Planetary Science Letters*, **12**, 97-107. https://doi.org/10.1016/0012-821x(71)90060-4

[32] Flower, M.F.J. (1973) Evolution of Basaltic and Differentiated Lavas from Anjouan, Comores Archipelago. *Contributions to Mineralogy and Petrology*, **38**, 237-260. https://doi.org/10.1007/bf00374768

[33] Barrat, J.A., Zanda, B., Jambon, A. and Bollinger, C. (2014) The Lithophile Trace Elements in Enstatite Chondrites. *Geochimica et Cosmochimica Acta*, **128**, 71-94. https://doi.org/10.1016/j.gca.2013.11.042

[34] Sun, S.S. and McDonough, W.F. (1989) Chemical and Isotopic Systematics of Oceanic Basalts: Implications for Mantle Composition and Processes. *Geological Society*, *London*, *Special Publications*, **42**, 313-345. https://doi.org/10.1144/gsl.sp.1989.042.01.19

[35] Cox, K.G., Bell, J.D. and Pankhurst, R.J. (1979) The Interpretation of Igneous Rocks. Unwin Hyman Ltd., 450 p.

[36] Aldanmaz, E., Pearce, J.A., Thirlwall, M.F. and Mitchell, J.G. (2000) Petrogenetic Evolution of Late Cenozoic, Post-Collision Volcanism in Western Anatolia, Turkey. *Journal of Volcanology and Geothermal Research*, **102**, 67-95. https://doi.org/10.1016/s0377-0273(00)00182-7

[37] Pearce, J.A. (2008) Geochemical Fingerprinting of Oceanic Basalts with Applications to Ophiolite Classification and the Search for Archean Oceanic Crust. *Lithos*, **100**, 14-48. https://doi.org/10.1016/j.lithos.2007.06.016

[38] Furman, T. and Graham, D. (1999) Erosion of Lithospheric Mantle beneath the East African Rift System: Geochemical Evidence from the Kivu Volcanic Province. *Lithos*, **48**, 237-262. https://doi.org/10.1016/s0024-4937(99)00031-6

[39] Ma, L., Jiang, S., Hofmann, A.W., Dai, B., Hou, M., Zhao, K., *et al*. (2014) Lithospheric and Asthenospheric Sources of Lamprophyres in the Jiaodong Peninsula: A Consequence of Rapid Lithospheric Thinning beneath the North China Craton? *Geochimica et Cosmochimica Acta*, **124**, 250-271. https://doi.org/10.1016/j.gca.2013.09.035

[40] Mbassa, B.J., Vanderhaeghe, O., Grégoire, M., Benoît, M., Itiga, Z., Ngwa Neh, C., *et al.* (2026) Sub-Continental Lithospheric Mantle beneath the Adamawa Volcanic Area (Cameroon Volcanic Line): Inference from Lavas and Hosted Mantle Xenoliths from Bini Warack, Ne-Ngaoundéré, Cameroon (Central Africa). *BSGF—Earth Sciences Bulletin*, **197**, Article 10. https://doi.org/10.1051/bsgf/2026005

[41] Wood, D.A. (1980) The Application of a Thhfta Diagram to Problems of Tectonomagmatic Classification and to Establishing the Nature of Crustal Contamination of Basaltic Lavas of the British Tertiary Volcanic Province. *Earth and Planetary Science Letters*, **50**, 11-30. https://doi.org/10.1016/0012-821x(80)90116-8

[42] Meschede, M. (1986) A Method of Discriminating between Different Types of Mid-Ocean Ridge Basalts and Continental Tholeiites with the Nb 1bZr 1bY Diagram. *Chemical Geology*, **56**, 207-218. https://doi.org/10.1016/0009-2541(86)90004-5

[43] Pearce, J.A. and Gale, G.H. (1977) Identification of Ore-Deposition Environment from Trace-Element Geochemistry of Associated Igneous Host Rocks. *Geological Society, London, Special Publications*, **7**, 14-24. https://doi.org/10.1144/gsl.sp.1977.007.01.03

[44] Shervais, J.W. (1982) Ti-V Plots and the Petrogenesis of Modern and Ophiolitic Lavas. *Earth and Planetary Science Letters*, **59**, 101-118. https://doi.org/10.1016/0012-821x(82)90120-0

[45] Condie, K.C. (2005) High Field Strength Element Ratios in Archean Basalts: A Window to Evolving Sources of Mantle Plumes? *Lithos*, **79**, 491-504. https://doi.org/10.1016/j.lithos.2004.09.014

[46] Condie, K.C. (2003) Incompatible Element Ratios in Oceanic Basalts and Komatiites: Tracking Deep Mantle Sources and Continental Growth Rates with Time. *Geochemistry, Geophysics, Geosystems*, **4**, 1-28. https://doi.org/10.1029/2002gc000333

[47] Bachelery, P. and Hémond, C. (2016) Geochemical and Petrological Aspects of Karthala Volcano. In: Bachelery, P., Lenat, J.F., Di Muro, A. and Michon, L., Eds., *Active Volcanoes of the Word*, Springer, 367-384.

[48] Ahamada, A., Cissokho, S., Labou, I., Diene, M., Oikifou, A.R. and Ngom, P.M. (2025) New Lithological, Petrographic and Geochemical Data from the Karthala Lava Massif, Grande Comore, Indian Ocean. *International Journal of Geosciences*, **16**, 204-223. https://doi.org/10.4236/ijg.2025.164011

[49] Clocchiatti, R., Havette Ledebt, A. and Nativel, P. (1979) Relations pétrogénétiques entre les basaltes transitionnels et les océanites du Piton de la Fournaise (île de la Réunion, océan Indien) à partir de la composition chimique des inclusions vitreuses des olivines et des spinelles. *Bulletin de Minéralogie*, **102**, 511-525. https://doi.org/10.3406/bulmi.1979.7300

[50] Valer, M. (2016) Origine et évolution des magmas de l'île de La Réunion: Apports de la pétro-géochimie et des inclusions magmatiques. Thèse de doctorat, Université Blaise Pascal, 362 p.

[51] Frey, F.A., Clague, D., Mahoney, J.J. and Sinton, J.M. (2000) Volcanism at the Edge of the Hawaiian Plume: Petrogenesis of Submarine Alkalic Lavas from the North Arch Volcanic Field. *Journal of Petrology*, **41**, 667-691. https://doi.org/10.1093/petrology/41.5.667

[52] Garcia, M.O., Caplan-Auerbach, J., De Carlo, E.H., Kurz, M.D. and Becker, N. (2006) Geology, Geochemistry and Earthquake History of Lȍihi Seamount, Hawaìi's Youngest Volcano. *Geochemistry*, **66**, 81-108. https://doi.org/10.1016/j.chemer.2005.09.002

[53] Thy, R. (1983) Phase Relations in Transitional and Alkali Basaltic Glasses from Iceland. *Contributions to Mineralogy and Petrology*, **82**, 232-251.

[54] Segar, M. (2013) Pétrogenèse des laves de l'île de la Possession (archipel de Crozet) et implications pour les hétérogénéités lithologiques des sources de points chauds. Thèse de Doctorat, Université de Nantes, 419 p.

[55] Cissokho, S., Ahamada, A., Ndiaye, A., Yatte, D. and Ngom, P.M. (2023) Contribution to the Petrographic and Geochemical Study of the Karthala Massif Lavas in the Bangaani Area, Grande Comore, Indian Ocean. *Open Journal of Geology*, **13**, 312-336. https://doi.org/10.4236/ojg.2023.135016

[56] Spāth, A., Roex, A.P.L. and Duncan, R.A. (1996) The Geochemistry of Lavas from the Gomores Archipelago, Western Indian Ocean: Petrogenesis and Mantle Source Region Characteristics. *Journal of Petrology*, **37**, 961-991. https://doi.org/10.1093/petrology/37.4.961

[57] Bourdon, B., Joron, J., Claude-Ivanaj, C. and Allègre, C.J. (1998) U-Th-Pa-Ra Systematics for the Grande Comore Volcanics: Melting Processes in an Upwelling Plume. *Earth and Planetary Science Letters*, **164**, 119-133. https://doi.org/10.1016/s0012-821x(98)00227-1

[58] Claude-Ivanaj, C., Bourdon, B. and Allègre, C.J. (1998) Ra-Th-Sr Isotope Systematics in Grande Comore Island: A Case Study of Plume-Lithosphere Interaction. *Earth and Planetary Science Letters*, **164**, 99-117. https://doi.org/10.1016/s0012-821x(98)00195-2

[59] Pelleter, A.A. (2013) L'île de Mayotte, archipel des Comores (France): Caractérisation pétrogéochimique des laves et pétrogèse des mélilitites à olivines. Volcanologie. Dumas-00854517.

[60] Rusquet, A., Famin, V., Quidelleur, X., Michon, L., Nauret, F., Danišík, M., *et al*. (2023) Pliocene-to-Holocene Volcano-Tectonic Activity on Mohéli Island (Comoros Archipelago) Constrained by New K Ar Ages. *Journal of Volcanology and Geothermal Research*, **442**, Article ID: 107896. https://doi.org/10.1016/j.jvolgeores.2023.107896